Mixed ionic-electronic conductivity and structural properties of strontium-borate glass containing nanocrystallites of $Bi_2VO_{5.5}$

N. A. Wójcik[*,1], **M. Prześniak-Welenc**[1], **P. Kupracz**[1], **J. Karczewski**[1], **M. Gazda**[1], **R. J. Barczyński**[**,1]

[1] Faculty of Applied Physics and Mathematics, Gdańsk University of Technology, Narutowicza Street 11/12, 80-233 Gdańsk, Poland

* Corresponding author: e-mail nwojcik@mif.pg.gda.pl, Phone: +48 58 348 66 06, Fax: +48 58 347 17 05

** e-mail jasiu@mif.pg.gda.pl, Phone: +48 58 347 18 32

Samples of strontium borate glass containing bismuth vanadate nanocrystallites were prepared. Nanocomposites containing up to 45 %mol of the $Bi_2VO_{5.5}$ phase exhibit electrical properties closer to the strontium-borate glass than to the ferroelectric $Bi_2VO_{5.5}$ ceramic. The glass matrix still may contain some part of bismuth and vanadium ions even after crystallization process and there is too little of crystalline phase to observe its ferroelectric properties. The glass-ceramic nanocomposite containing 50 %mol of $Bi_2VO_{5.5}$ phase exhibits electrical properties closer to the $Bi_2VO_{5.5}$ ferroelectric. The electric parameters of conduction processes in the $Bi_2VO_{5.5}$ nanocrystallites, glass matrix and phases boundaries are discussed. The conduction process mechanism in all nanocomposites for the low temperatures is mixed ionic-electronic and in the higher temperatures the oxygen ion hopping starts to dominate.

1 Introduction Ferroelectric glass-ceramic nanocomposites show unique physical properties which may be used in certain electronic applications. Electric parameters of such nanocomposites mostly depend on quantity and size of dispersed crystallites as well as phase boundaries occurrence [1-6]. Therefore in order to receive ferroelectric nanocomposites it is important to select appropriate content of both glassy and crystalline phases and crystallization process parameters.

One of ferroelectric ceramics which may be dispersed in a glass matrix is $Bi_2VO_{5.5}$ (BiV) [7-9]. This ceramic exhibits two first order phase transitions α↔β phase at 730 K and β↔γ phase at 835 K. All three main polymorphs of BiV contain oxygen ion vacancies in the V-O layers which give rise to the high ionic D.C. conductivity of an order of $10^{-6} \ \Omega^{-1} \cdot cm^{-1}$ at 730 K and $10^{-3} \ \Omega^{-1} \cdot cm^{-1}$ at 923 K [10-14].

The strontium-borate glass (SBO) is a promising host matrix for dispersing ferroelectric crystallites and can be easily prepared by the traditional melting method [15-17]. It shows rather high value of electric permittivity about 14 and low D.C. conductivity of an order of $10^{-12} \ Scm^{-1}$ (at 813 K). The conduction mechanism of this material is oxygen vacancies hopping [17].

There are some studies on the properties and structure of composites of the bismuth vanadate (BiV) with glasses [17-23]. However the structural and thermal measurements results of these materials presented in [18-23] are not coherent and only basic information about electrical permittivity behavior is included.

The aim of this work is to find the appropriate amount of crystalline phase and optimal crystallite size necessary to obtain ferroelectric properties in $Bi_2VO_{5.5}$-SrB_4O_7 system. There is a lack of detailed knowledge of the electrical behavior of these materials. Our goal is to determine the mechanism and electric parameters of conduction processes in the $Bi_2VO_{5.5}$ nanocrystallites, glass matrix and phases boundaries. For this purpose an analysis of A.C. permittivity and conductivity of obtained glass-ceramic nanocomposites and the $Bi_2VO_{5.5}$ ceramic as well as strontium-borate glass will be performed.

2 Experimental In order to prepare glass-ceramics composites two compounds: $Bi_2VO_{5.5}$ and SrB_4O_7 were synthesized via a solid state reaction route. The $Bi_2VO_{5.5}$ was synthesized from the stoichiometric mixture of initial powders of Bi_2O_3 and V_2O_5 which were ball-milled in pure acetone for 6 h at room temperature. The milling was performed in steps of 1 h with rest intervals of 10 min. The mixture was heated up to 1020 K in air and kept at this temperature for 24 h. The heating and cooling rate was of 50 $K.h^{-1}$. The obtained powder was checked by X-ray diffraction method. It can be seen that it consists of one phase $Bi_2VO_{5.5}$ (Fig. 1). The SrB_4O_7 was synthesized from the stoichiometric mixture of analytical grade $SrCO_3$ and H_3BO_3 which were mashed in a mortar. Next the mixture was heated up to 1073K and kept at this temperature for 12 hours.
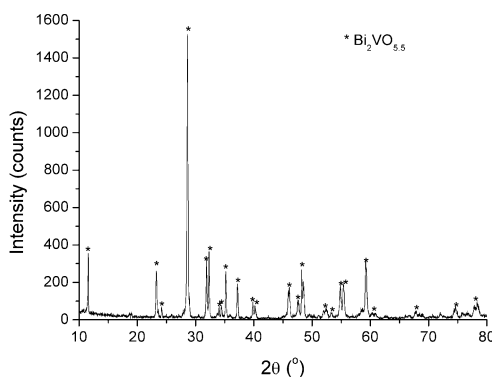

Figure 1 XRD pattern of $Bi_2VO_{5.5}$ powder at room temperature.

Samples of a composition of $xBi_2VO_{5.5}$-$(100-x)SrB_4O_7$, where x=30, 35, 40, 45 and 50 (in %mol) were prepared by the conventional melt quenching technique. The melting was conducted in alumina crucibles at 1373 K for 2 hours. The melts were poured onto a preheated (573 K) brass plate and pressed by another plate to obtain flat circular disks of 1-2 mm thickness and 20-30 mm diameter. In the following, sample symbols were simplified to xBiV(100-x)SBO. Their compositions and short names are listed in Tab. 1. In addition, a $Bi_2VO_{5.5}$ ceramic sample was prepared for comparison.

The color of as-quenched samples changes with the increase in amount of $Bi_2VO_{5.5}$ phase from light to dark brown and their transparency decreases. All materials were crystallized in order to obtain glass-ceramics nanocomposites. The crystallization temperature was determined on the basis of DSC curves. Samples were heat-treated at 813 K for 3 hours. During the crystallization the samples darkened and their transparency was reduced. It was impossible to prepare physically stable samples containing more than 50 %mol of BiV phase because they easily broke during quenching and heat-treatment.

The structure was studied by the X-ray diffraction (XRD) method with a Philips X 'Pert Pro MPD system with the CuKα radiation. Differential scanning calorimetry (DSC) measurements were performed on powdered samples in a flow of nitrogen at 50 cm^3min^{-1} using a Netzsch STA 449F1 thermal analyser. The heating rate was maintained at 15 $K.min^{-1}$ within a temperature range of 373–913 K. The topography of the samples was investigated using a Scanning Electron Microscope (SEM), FEI Company Quanta FEG250 with Energy Dispersive X-ray Analysis (EDAX Genesis APEX 2i with Apollo x SDD Spectrometer). SEM measurements were conducted on fractured samples on which a 7 nm thick gold layer was deposited, using a 10 or 20kV beam accelerating voltage with a SE-ETD (secondary electron - Everhart-Thornley detector) detector working in the high vacuum mode (pressure 10^{-4} Pa).

For electrical measurements gold electrodes were evaporated onto the surface of the polished samples. Linear impedance measurements were carried out in air in a frequency range from 10 mHz to 1 MHz with an A.C. voltage of 1 V_{rms} in the temperature range from 373 to 813 K with a step of 10 K using a Novocontrol Concept 40 broadband dielectric spectrometer and high temperature Novotherm HT 1600 Controller. The measurements were carried out during both increasing and decreasing temperature.
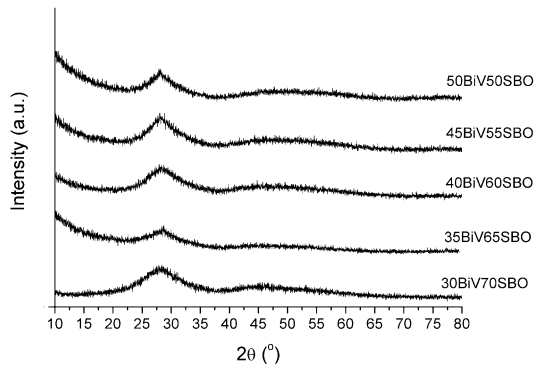
3 Results
3.1 Structure and morphology The XRD patterns for all as-quenched samples are shown in Fig. 2a. There is a broad X-ray peak around 28° which suggests the existence of nanocrystalline phase in all as-quenched samples. The results for all samples after the crystallization process are presented in Fig. 2b. It may be seen that some reflections of the $Bi_2VO_{5.5}$ crystalline phase are visible in all crystallized samples. Their intensity increases and broadness decreases with an increase in BiV amount.

Figure 3 shows as example the DSC curve obtained for the as-quenched 50BiV50SBO sample. The results obtained for the samples containing from 35 to 50 %mol of
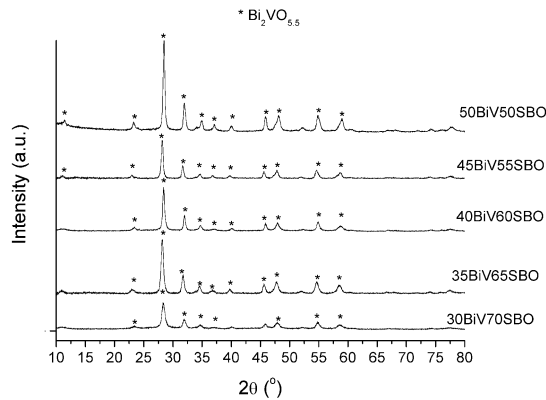
BiV were similar. They showed one exothermic and one endothermic process. The sample containing 30 %mol of $Bi_2VO_{5.5}$ exhibits only one endothermic process. The temperatures of exo-/endothermic processes for all measured materials are listed in Tab. 1. The glass transition temperatures are hard to determine reliably because of visible noise.

(a)

(b)

Figure 2 XRD pattern of **(a)** as-quenched and **(b)** heat-treated samples at room temperature.

Table 1 Summary of DSC results for all samples: exo- and endothermic processes temperatures.

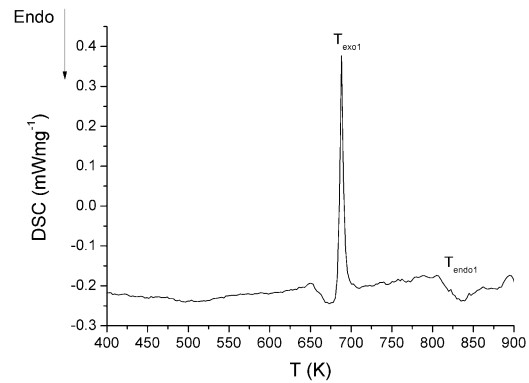| Sample composition Short name	T_{exo} (K)	T_{endo1} (K)	T_{endo2} (K)
$30Bi_2VO_{5.5}$-$70SrB_4O_7$ *30BiV70SBO*	-	837	-
$35Bi_2VO_{5.5}$-$65SrB_4O_7$ *35BiV65SBO*	686	829	
$40Bi_2VO_{5.5}$-$60SrB_4O_7$ *40BiV60SBO*	677	842	-
$45Bi_2VO_{5.5}$-$55SrB_4O_7$ *45BiV55SBO*	681	824	-
$50Bi_2VO_{5.5}$-$50SrB_4O_7$ *50BiV50SBO*	688	845	-
$Bi_2VO_{5.5}$ *BiV [14]*	-	715	841

Figure 3 An example of DSC curve for as-quenched 50BiV50SBO sample.

Figure 4 presents examples of SEM images of fractured as-quenched samples containing (a) 30, (b) 40 and (c) 50 %mol of the BiV phase. The SEM results for other 35BiV65SBO and 45BiV55SBO samples are similar to 40BiV60SBO one. It can be seen that all glass materials, exhibit a specific nanostructure. An increase in the BiV phase from 30 to 45 %mol, slightly increases the size of the visible structures. For 50BiV50SBO sample the change in the surface topography is more noticeable. EDS results confirmed the average amount of bismuth, vanadium, strontium and boron but small traces of aluminium were also detected. The origin of these impurities may be from alumina crucibles used.
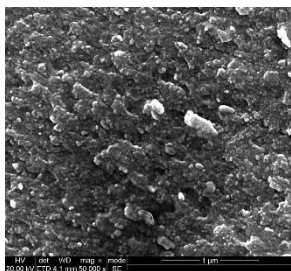
(a) **(b)**
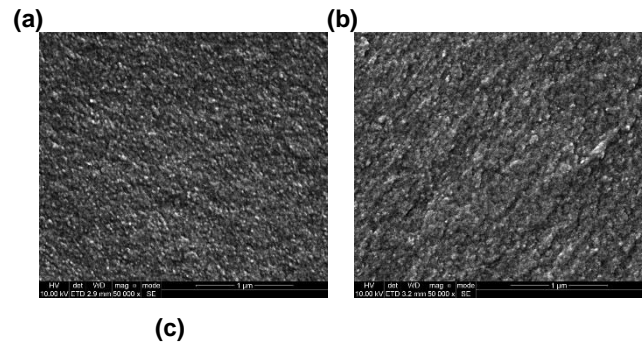
(c)

Figure 4 The examples of SEM pictures of fractured as-quenched **(a)** 30BiV70SBO, **(b)** 40BiV60SBO and **(c)** 50BiV50SBO samples (in %mol) for 50 000x magnitude and SE-detector.

The morphology of all samples changed after the crystallization process. Figures 5a, 5b and 5c show examples of SEM pictures of the heat-treated 30BiV70SBO, 40BiV60SBO and 50BiV50SBO samples, respectively. There is no distinct difference between samples containing up to 45 %mol of BiV phase. The crystallization process increased the size and amount of visible nanostructures.
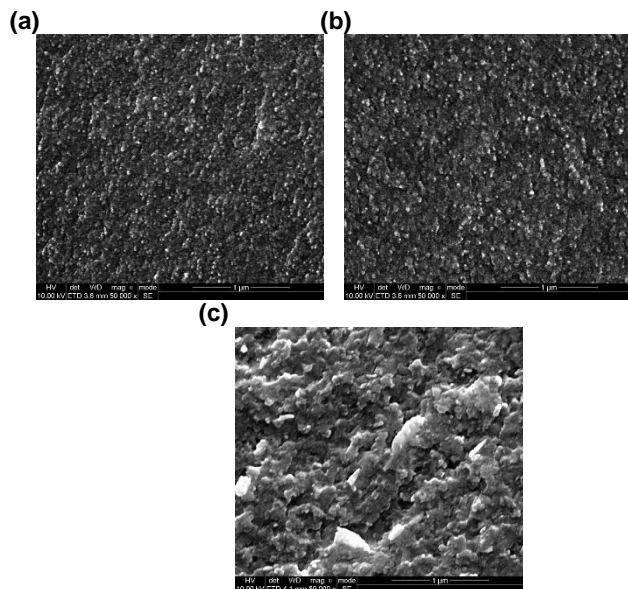

Figure 5 The examples of SEM pictures of fractured heat-treated **(a)** 30BiV70SBO, **(b)** and 40BiV60SBO **(c)** 50BiV50SBO samples (in %mol) for 50 000x magnitude and SE-detector.

3.2 Electrical properties Figure 6a shows the temperature dependence of the real part of A.C. conductivity at 10Hz (the middle point of frequency range) for all samples. The results obtained during heating and cooling cycles were marked by arrows. It may be seen that all samples containing up to 45 %mol of BiV phase exhibit similar conductivity behavior during the first heating-cooling cycle. The 50BiV50SBO sample (crosses) during the first heating-cooling cycle shows significantly different trend of conductivity curve than the other materials. During the first

heating the conductivity of the 50BiV50SBO sample exhibits a minimum near temperature of 653 K whereas above 683 K (T_{exo1}) it shows a monotonic increase. The cooling curve of this sample presents conductivity values higher than these in the first heating. The conductivity of this material is significantly higher than that of the other samples.

The temperature dependence of the real part of electric permittivity at 10 Hz for all samples is displayed in Fig. 6b (the first heating-cooling cycle). It may be seen that materials containing up to 45 %mol of BiV phase show similar values of electric permittivity (from 9 to 23). The 50BiV50SBO sample (crosses) shows the electric permittivity significantly higher than the other materials. During the first heating its permittivity increases with temperature and between 640 K do 700 K a rapid increase of more than two orders of magnitude is visible. It achieves the maximum value of the order of 10^5. During the cooling, the permittivity of this sample monotonically decreases. The behavior of its electric parameters (conductivity and permittivity) was the same during the cooling and subsequent measurements.
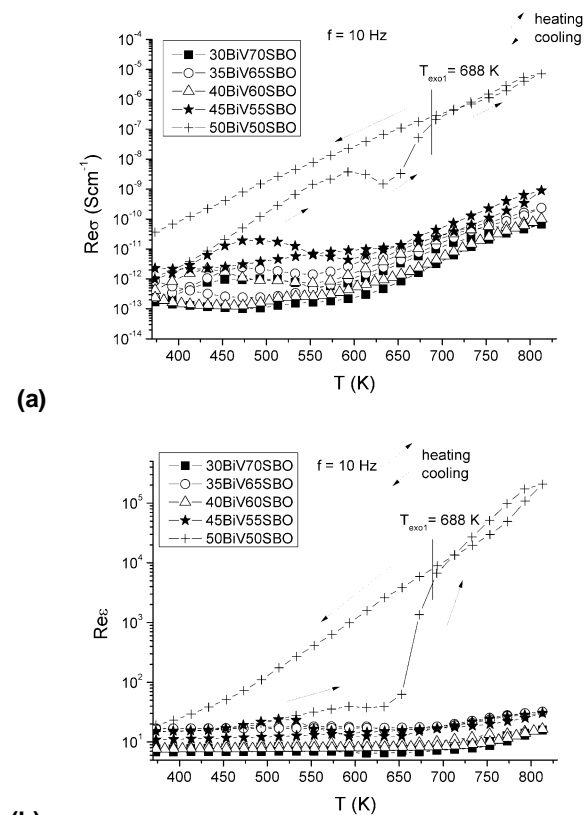

(a)

(b)

Figure 6 The temperature dependence of the real part of **(a)** A.C. conductivity and **(b)** electric permittivity at 10 Hz for all samples.
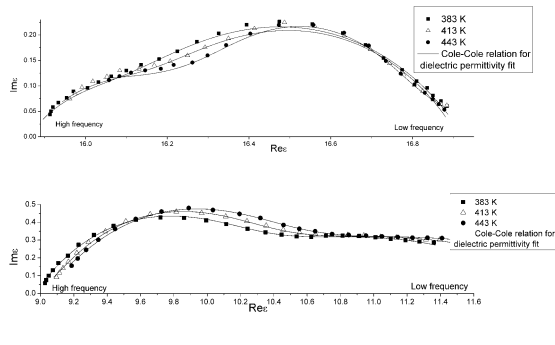
(a)

(b)

Figure 7 The Cole-Cole plots for **(a)** 35BiV65SBO and **(b)** 45BiV55SBO glass-ceramics nanocomposites.

Figure 7 displays an examples of Cole-Cole plots for 35BiV65SBO (Fig. 7a) and 45BiV55SBO (Fig. 7b) glass-ceramics nanocomposites. All samples containing less than 50 %mol of BiV phase show similar behavior. For these materials two relaxation processes are visible in the low temperature region. The 50BiV50SBO sample did not show any distinctive semicircles in Cole-Cole plots.
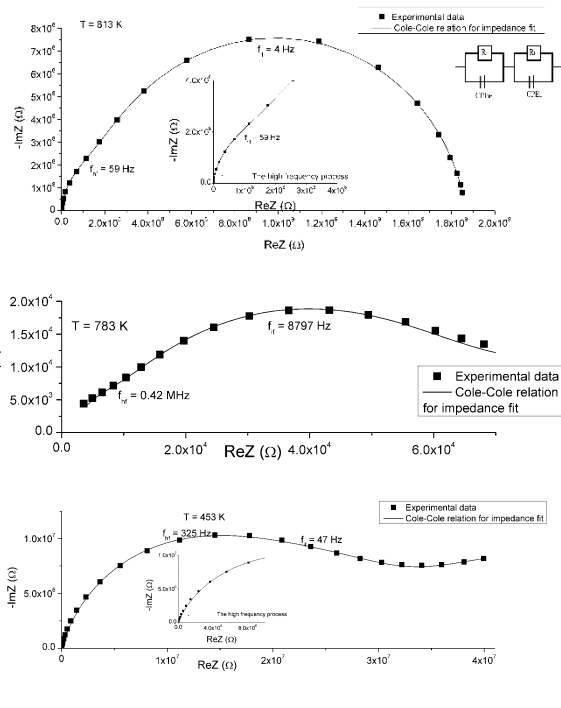

(a)

(b)

(c)

Figure 8 The imaginary part versus real part of impedance (the Nyquist plot) for **(a)** 30BiV70SBO, **(b)** 50BiV50SBO glass-ceramics nanocomposites and **(c)** BiV ceramic. The solid lines in the picture represent the results of fitting.

Figure 8 presents an examples of Nyquist plots (imaginary versus real part of the impedance) for 30BiV70SBO (Fig. 8a) and 50BiV50SBO (Fig. 8b) glass-ceramics nanocomposites. The Nyquist plots for all glass-ceramics nanocomposites consist of two (BiV phase content $\leq$ 35 %mol)

or three (BiV phase content $\geq$ 40 %mol) overlapping semicircles. They correspond to two or three relaxation processes. Figure 8c presents the Nyquist plot for BiV ceramic in order to facilitate the comparative analysis. Impedance spectra for this ceramic show two relaxation processes in the low temperature range. There may be also seen the onset of the third relaxation process which starts to dominate in the higher temperatures (above 643 K).

4 Discussion

4.1 Structure and morphology All samples even directly after preparation contain traces of nanocrystalline phase. The heat-treatment results in formation of clearly detectable $Bi_2VO_{5.5}$ nanocrystallites in all tested materials. In order to estimate $Bi_2VO_{5.5}$ crystallite size the line profile analysis on the two strongest reflections observed in XRD diffraction patterns was performed. Figure 9 presents the crystallite size as a function of BiV phase content. The obtained crystallite size is between 15 and 40 nm and it increases with the BiV amount. The heat-treated 50BiV50SBO sample exhibits the highest amount of BiV with a mean crystallite size of about 40 nm. The crystallization of BiV is observed from about 680 K (exothermic process visible in DSC curve in Fig. 3). Electrical properties suggest that some changes in the samples structure take place up to a temperature of 813 K, close to the endothermic process which may be correlated with the second $\beta \leftrightarrow \gamma$ phase transition of BiV (in 814 K) [14].
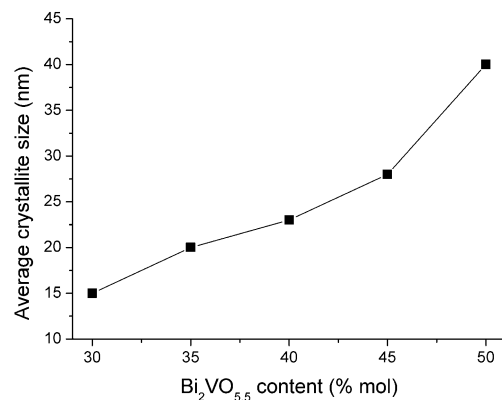
Figure 9 The average crystallite size as a function of BiV content in samples.

The available literature about similar materials [18-20] is not coherent. Materials tested in this work does not show exothermic processes above 700 K, in contrast to what was observed in N. Syam Prasad et al. work [18]. In all glass-ceramics nanocomposites the $\beta \leftrightarrow \gamma$ phase transition of BiV was detected, which was not observed before. No additional crystalline phase was observed in contrast to N. Syam Prasad et al. observations [18] and average BiV crystallites size is higher than obtained in [18-20].

4.2 Complex impedance The analysis of different dielectric functions such as: complex electric permittivity ε^*, complex impedance Z^* and complex conductivity σ^* may allow us to link the electrical parameters with the microstructure of studied materials [24].

Modeling of the relaxation processes observed in Nyquist plots may be carried out using different empirical relations: Debye, Cole-Cole, Cole-Davidson and Havriliak-Negami [25]. The best fitting results of the experimental data analyses were obtained with a superposition of two or three Cole-Cole relaxation processes. This model allows to separate the components of the conductivity processes taking place through the different composite regions: the crystalline phase and the amorphous matrix. The Cole-Cole expression for impedance describes an equivalent circuit consisting of a resistance and a CPE element connected parallel, and is given by [26]:

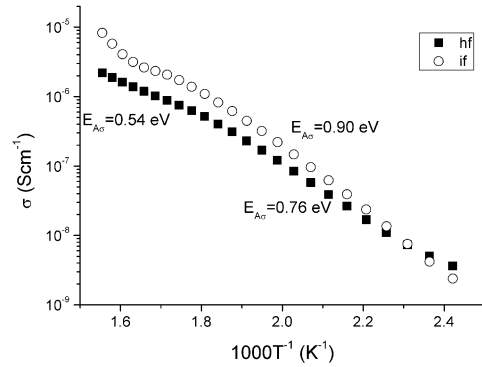$$Z^* = \frac{R}{1+(j\omega\tau_{RPCE})^{1-\alpha}} \qquad (1)$$

where Z^* is the complex impedance, R is the equivalent resistance of a process, τ_{RCPE} is the mean dielectric relaxation time, ω $(=2\pi f)$ is an angular frequency and α is a parameter which describes the width of the relaxation time distribution.
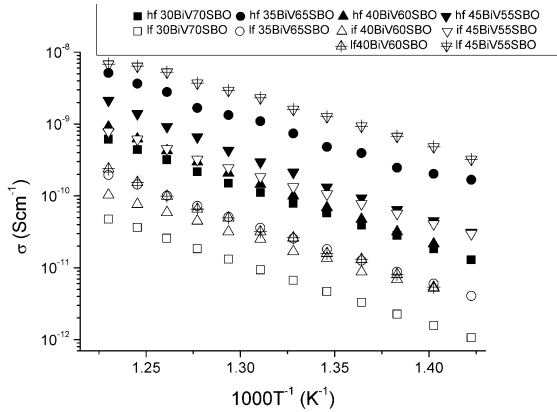
(a)
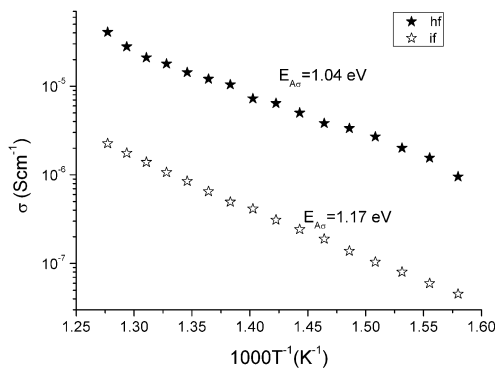
(b)

(c)

Figure 10 The temperature dependence of the conductivity calculated with the use of Cole-Cole relation for impedance for **(a)** glass-ceramics nanocomposites containing up to 45 %mol of BiV phase, **(b)** 50BiV50SBO glass-ceramic nanocomposite and **(c)** BiV ceramic. Symbols: hf - high frequency process, if – intermediate frequency process, lf – low frequency process.

The solid lines in figures 8a, b and c show the results of Cole-Cole relaxations fitting to the experimental data. In the 50BiV50SBO nanocomposite and the BiV ceramic only the onset of the third low frequency process is visible and there is impossible to reliably fit it to relaxation equation. In all glass-ceramics nanocomposites the process proceeded in the high frequency region, shows a close to Debye-type character ($\alpha\approx0$). The conductivities were calculated from resistances determined using relation (1).

Figures 10a, b and c show the temperature dependence of the conductivity for 30BiV70SBO (squares), 35BiV65SBO (circles), 40BiV60SBO (triangles), 45BiV55SBO (upside-down triangles), 50BiV50SBO glass-ceramics nanocomposites and BiV ceramic. The relaxation time for thermally activated relaxation is described by the expression [27]:

$$\tau = \tau_0\exp(\frac{E_{A\tau}}{kT}) \qquad (2)$$

where: τ_0 is the relaxation time at an infinite temperature and $E_{A\tau}$ is the activation energy.

The activation energy of conduction processes were evaluated using the Arrhenius relation:

$$\sigma T = \sigma_0\exp(\frac{E_{A\sigma}}{kT}) \qquad (3)$$

where σ_0 is a constant. Table 2 presents activation energy of conduction processes. The α parameter is displayed for all glass-ceramics nanocomposites in Fig. 11a and for BiV ceramic in Fig. 11b.

The BiV ceramic shows the activation energy of both conduction processes between 0.9 and 0.5 eV depending on the temperature region. It is known that the lower the α parameter, the narrower the distribution of the relaxation

time is, and the more ordered the structure is [26]. The structure of crystallites is more ordered than the structure between them, therefore lower values of the α dispersion parameter suggests that the high frequency process is due to conduction process within crystallites. The intermediate frequency process in such a case would be connected with the phases between crystallites (boundaries). The third process proceeding in the lowest frequency region may be related with the space charge accumulation, which is usually visible in the high temperatures and shows high values of relaxation time. In the BiV two conduction mechanisms are possible. The first one is polaron hopping (electron with the accompanying local lattice deformation) hopping from transition metal ion at lower V^{4+} to neighboring ion at higher oxidation level V^{5+} [28]. The second one is ion hopping of oxygen vacancies, dominating in the higher temperature region (above 553 K).

(a)

(b)
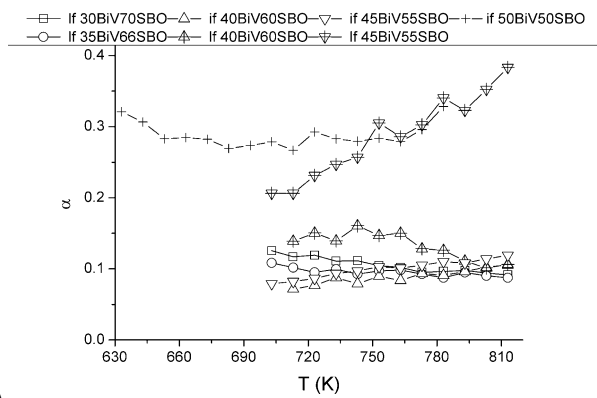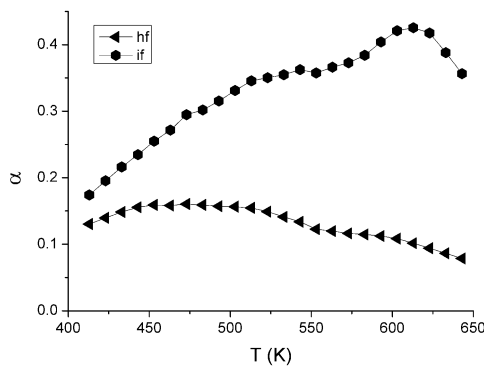
Figure 11 The α dispersion parameter for **(a)** all glass-ceramics nanocomposites and **(b)** BiV ceramic. Symbols: hf - high frequency process, if – intermediate frequency process, lf – low frequency process.

Table 2 The activation energy of conduction processes for all heat-treated samples. T_l means temperature range 393-593 K and T_h 563-643 K.

Short name	Conduction process	$E_A(\tau)$ (eV)	$E_A(\sigma)$ (eV)		
30BiV70SBO	The high frequency	1.79	1.79		
	The low frequency	1.66	1.77		
35BiV65SBO	The high frequency	1.73	1.64		
	The low frequency	1.69	1.79		
40BiV60SBO	The high frequency	1.78	1.92		
	The intermediate frequency	1.59	1.58		
	The low frequency	1.56	1.90		
45BiV55SBO	The high frequency	1.79	1.95		
	The intermediate frequency	1.62	1.53		
	The low frequency	0.64	1.46		
50BiV50SBO	The high frequency	1.08	1.04		
	The intermediate frequency	1.13	1.17		
		T_l	T_h	T_l	T_h
BiV	The high frequency	0.78	0.57	0.76	0.54
	The intermediate frequency	0.59	-	0.90	-

The glass-ceramics nanocomposites containing up to 45 %mol of BiV phase exhibit the activation energy of conduction processes between 1.5 and 2 eV. Whereas the both, low- and high frequency processes for the 50BiV50SBO sample are described by significantly lower activation energy (about 1 eV). In all glass-ceramics nanocomposites the dispersion parameter α for the high frequency process is practically 0. The other processes in the intermediate and low frequency regions show higher values of the α parameter. The fastest process in all nanocomposites (practically Debye relaxation) is due to conduction process through the nanocrystallites of $Bi_2VO_{5.5}$ phase (the most ordered structure). The low frequency process observed in samples containing up to 35 %mol of BiV phase

is characterized by similar parameters to the intermediate frequency process visible in materials with the BiV phase content more than 35 %mol. This process may occur within the residual glass matrix. The third process in the lowest frequency region detected in 40BiV60SBO, 45BiV55SBO and 50BiV50SBO samples may be related to space charge accumulation. For nanocomposites containing up to 45 %mol of BiV phase the relatively high activation energy and temperature of all the processes occurrence suggest ion hopping. The 50BiV50SBO glass-ceramic nanocomposite shows a large increase in conductivity and decrease in activation energy of the both processes in the comparison to the other nanocomposites. This change may be caused by an increase in BiV crystalline phase content and development of an additional conduction mechanism – polaron hopping. Only this sample exhibits electrical behavior similar to the BiV ceramic.

4.3 A.C. and D.C. conductivity The conductivity of many dielectric systems may be described by Jonscher power law called UDR 'Universal dielectric response' expressed by relation [25, 29, 30]:

$$\sigma'(\omega) = \sigma_{DC}(T) + A(T)\omega^{s(T)} \quad (4)$$

where: $\sigma'(\omega)$ is the real part of total conductivity, σ_{DC} is the frequency independent (D.C.) conductivity and the coefficient A and exponent s ($0<s<1$) depend on temperature and material properties. The term $A\omega^s$ contains the A.C. dependence and characterizes dispersion. Later also conductive systems began to be modelled using this formula and the UDR abbreviation has been extended to 'Universal dynamic response' [31, 32]. S. Kumar et. al [33] proposed a different method for the conductivity spectrum analysis - double power law. They found that for materials in which apart from frequency independent plateau region, the conductivity spectrum consists of two dispersions in the A.C. region, the A.C. conductivity fulfills relation:

$$\sigma'(\omega) = \sigma_{DC} + A_{lf}(T)\omega^{s_{lf}(T)} + A_{hf}(T)\omega^{s_{hf}(T)} \quad (5)$$

where the exponent $0<s_{lf}<1$, characterizes the low-frequency dispersion corresponding to the translation ion hopping and the exponent $1<s_{hf}<2$ characterizes the high frequency dispersion, indicating the existence of well localized relaxation process [33].
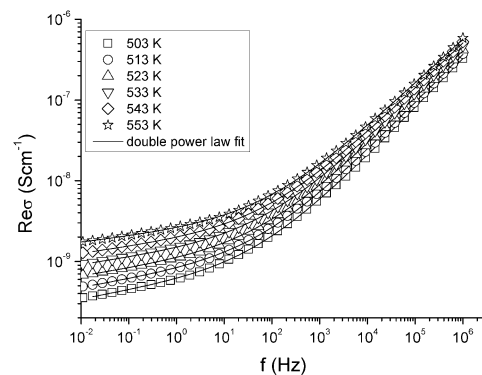
Figure 12 displays the frequency dependence of the real part of A.C. conductivity at several temperatures for 45BiV55SBO (Fig.12a) and 50BiV50SBO (Fig. 12b) glass-ceramics nanocomposites. The samples A.C. conductivity shows good agreement with double power law only at temperatures in which relaxation processes are not visible. The solid lines represent the results of equation (5) fitted to experimental data. The s_{hf}, s_{lf} dispersion parameters as a function of temperature for glass-ceramics nanocomposites and BiV ceramic are presented in Fig. 13. In

45BiV55SBO nanocomposite in A.C. conductivity curves the relaxation processes are present in all temperature range and fitting is impossible.

In the BiV ceramic the high frequency dispersion is attributed by impedance analysis to conduction process within crystallites. Its s_{hf} dispersion parameter increases to 1 with an increase in temperature. Literature data of ionic conductors [34] suggests that materials with high concentration of mobile ions are characterized by s dispersion parameter of about $0,5–0,6$. In a such situation it may be suggested that the concentration of mobile ions in crystallites is rather high. We believe that in the BiV ceramic the low frequency dispersion is due to conduction process within crystallites boundaries which is assigned to intermediate frequency process visible in impedance analysis. The BiV ceramic in the low frequency range shows dispersion exponent s_{lf} almost temperature independent with value of 0.1. H. Jain et. al [34] suggest that $s \rightarrow 0$ when the mobile ions concentration approaches zero. In such a case this region is poor in mobile ions and ion hopping within it is limited.
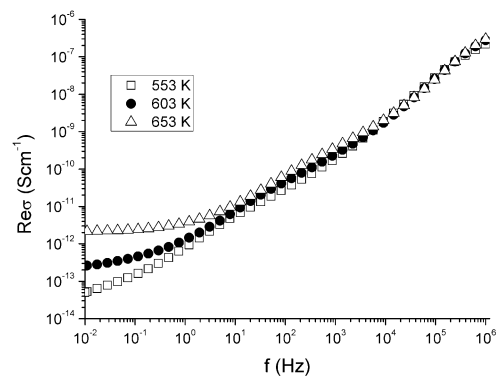
(a)

(b)

Figure 12 The frequency dependence of the real part of A.C. conductivity at several temperatures for **(a)** 45BiV55SBO and **(b)** 50BiV50SBO glass-ceramics nanocomposites.
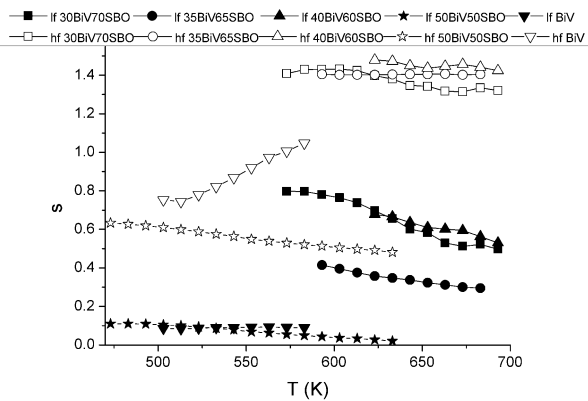
Figure 13 The temperature dependence of *s* dispersion parameter for glass-ceramics nanocomposites and BiV ceramic. Symbols: hf - high frequency dispersion, lf – low frequency dispersion.

In nanocomposites containing up to 40 %mol of BiV phase both high and low frequency dispersions exhibit similar values of *s* dispersion parameter. Two dispersions may be correlated with conduction process within two regions respectively: $Bi_2VO_{5.5}$ nanocrystallites and surrounding glass matrix. The situation in 50BiV50SBO glass-ceramic nanocomposite is similar to BiV ceramic: it shows *s* exponent values for the both dispersions significantly lower than the other nanocomposites; the high frequency dispersion is correlated with conduction process within BiV nanocrystallites which contain high concentration of mobile ions; the low frequency dispersion is correlated with glass matrix and phases boundaries which are poor in mobile ions.
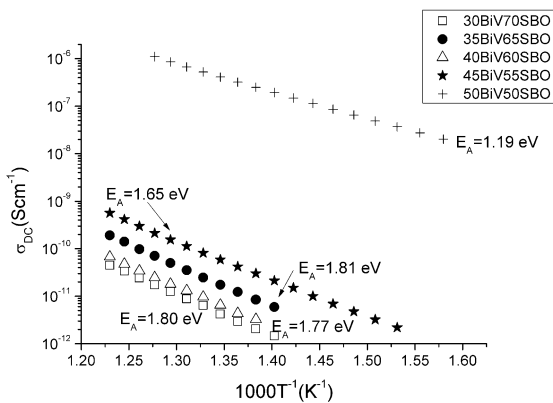

Figure 14 The D.C. conductivity versus 1000/T with activation energy for all glass-ceramics nanocomposites.

Figure 14 shows D.C. conductivity versus the reciprocal of the temperature for all glass-ceramics nanocomposites. These values were calculated from a low frequency plateau. The activation energy was calculated with the use of Arrhenius relation (3). It may be seen that the D.C. con-

ductivity increases and activation energy decreases with the increase in BiV quantity. The activation energy of D.C. conductivity for all glass-ceramics nanocomposites has values typical for ionic conduction mechanism. Literature data shows that strontium-borate glass exhibits rather low values of D.C. conductivity (an average order of magnitude of 10^{-12} Scm^{-1} at 753 K with $E_A = 1.51$ eV) and its conduction mechanism is due to oxygen vacancies [17]. The BiV ceramic shows D.C. conductivity significantly higher than SBO glass (from an order of magnitude of 10^{-4} Scm^{-1} at 913 K with $E_A = 1.27$ eV to 10^{-10} Scm^{-1} at 503 K with $E_A = 0.57$ eV) [14].

The glass-ceramics nanocomposites containing up to 45 %mol of BiV phase shows D.C. conductivity and its activation energy closer to strontium-borate glass than to BiV ceramic. The D.C. conduction process in all studied nanocomposites may be caused by oxygen vacancies occurring in the both glass matrix and $Bi_2VO_{5.5}$ nanocrystallites. For the 50BiV50SBO sample may be seen that the BiV phase has dominant influence on its conductivity and lower activation energy suggests an additional conduction mechanism appearance – the polaron hopping.

4.4 Complex electric permittivity The 50BiV50SBO glass-ceramic nanocomposite shows a rapid increase in electric permittivity above 652 K (Fig. 6b) which is close to the ferro-paraelectric phase transition, characteristic for the BiV phase [14]. Therefore this observed change may be due to the phase transition. At the same time the conductivity significantly increases what may also induce similar effect on account of the space charge accumulation. For the other studied materials their electric permittivity is closer to this of a strontium-borate glass [17].

The complex electric permittivity (Fig. 7) was fitted using the sum of two Cole-Cole relations which describes the polydispersive nature of the dielectric relaxation. The Cole–Cole distribution for electric permittivity for each process may be written as [25]:

$$\varepsilon^* = \varepsilon_\infty + \frac{\varepsilon_s - \varepsilon_\infty}{1 + (j\omega\tau\varepsilon)^{1-\alpha}} \qquad (6)$$

where ε^* is the electric permittivity, ε_s and ε_∞ are the static and high-frequency limiting electric permittivity for the process, τ_ε is the mean dielectric relaxation time, and α is a parameter lower than 1 [25]. The solid lines in Fig. 7 show the fitting results.
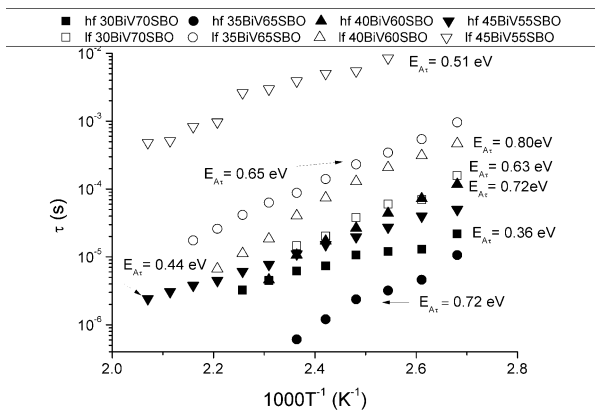
Figure 15 The temperature dependence of the mean relaxation time of dielectric loss for all glass-ceramics nanocomposites containing up to 45 %mol of BiV phase. Symbols: hf - high frequency relaxation process, lf – low frequency relaxation process.

Figure 15 displays the mean relaxation time of the dielectric polarization processes versus temperature for glass-ceramics nanocomposites containing up to 45 %mol of BiV phase. The activation energy was calculated using Arrhenius relation (2). In almost all samples the high frequency process is described by the lower activation energy than the low frequency one. The calculated values of activation energy in analyzed materials have possible physical meaning for the both polaron and ion hopping.

5 Conclusions All as-quenched $xBi_2VO_{5.5}$-(100-x)SrB_4O_7 samples contain nanocrystalline phase. After heat-treatment the size and amount of detected $Bi_2VO_{5.5}$ nanocrystallites increase. The crystallization process of this phase was observed from temperature of about 680 K up to 813 K. In all materials the second $\beta \rightarrow \gamma$ phase transition of crystallized phase is visible at about 830 K.

On the basis of electrical properties analysis it is suggested that all nanocomposites with the exception of $50Bi_2VO_{5.5}$-$50SrB_4O_7$, despite the presence of $Bi_2VO_{5.5}$ crystalline phase, show electrical properties closer to the strontium-borate glass. Contrary to expectation, the behavior typical for ferroelectrics was not observed. It is suggested that in these materials, some part of the bismuth and vanadium oxides still play a role of glass formers and built the glass matrix even after crystallization process. The glass-ceramics nanocomposites show two or three dispersion processes for the complex impedance, conductivity and complex electric permittivity. It is suggested that the fastest process is correlated with conduction process through the $Bi_2VO_{5.5}$ nanocrystallites, the others two processes are associated with the residual glass matrix or the space charge accumulation. The conduction process mechanism for the low temperatures may be mixed ionic-electronic and in the higher temperatures the oxygen ion hopping starts to dominate.

The $50Bi_2VO_{5.5}$-$50SrB_4O_7$ glass-ceramic nanocomposite is the only one which exhibits the electrical properties similar to the $Bi_2VO_{5.5}$ ferroelectric. It presents significantly higher conductivity and electric permittivity. It shows two dispersion processes. The faster one is assigned to the conduction through the $Bi_2VO_{5.5}$ nanocrystallites and is due to the high concentration of the mobile ions. The other dispersion may be associated with the glassy phase surrounding nanocrystallites and phase boundaries. It is shown that in these regions the mobile ions concentration is low.

References

[1] Neelam Kumari, S.B. Krupanidhi, K.B.R. Varma, Mat. Sci. Eng. B **138**, 22 (2007).
[2] S.J. Skinner, J.A. Kilner, Mater. Today **6**, 30 (2003).
[3] M.S. Al-Assiri, M.M. El-Desoky, A. Al-Hajry, A. Al-Shahrani, A.M. Al-Mogeeth, A.A. Bahgat, Physica B **404**, 1437 (2009).
[4] S. Ezhilvalavan, J.M. Xue,Wang John:, Mater. Chem. Phys. **75**, 50 (2002).
[5] A.M. Glass, M.E. Lines, K. Nassau, J.W. Shiever, Appl. Phys. Lett. **31**, 249 (1977).
[6] N.V. Golubev, V.N. Sigaev, S.Yu. Stefanovich, T. Honma, T. Komatsu, J. Non-Cryst. Solids **354**, 1909 (2008).
[7] A.A. Bush, Yu.N. Venevtsev, Russ. J. Inorg. Chem. **31** (5), 769 (1986).
[8] N. Kumari, S.B. Krupanidhi, K.B.R. Varma, Mater. Sci. Eng. B **138**, 22 (2007).
[9] G. Paramesh, N. Kumari, S.B. Krupanidhi, K.B.R. Varma, Opt. Mater. **34**, 1822 (2012).
[10] F. Abraham, M.F. Debreuille- Gresse, G. Mairesse, G. Nowogrocki, Solid State Ionics **28–30**, 529 (1988).
[11] F. Abraham, J.C. Boivin, G. Mairesse, G. Nowogrocki, Solid State Ionics **40–41**, 934 (1990).
[12] K.B.R. Varma, G.N. Subbanna, T.N. Guru Row, C.N.R. Rao, J. Mater. Res. **5**, 2718 (1990).
[13] K.V.R. Prasad, K.B.R. Varma, J. Mater. Sci. 30 (1995) 6345.
[14] N.A. Szreder, P. Kupracz, M. Prześniak-Welenc, J. Karczewski, M. Gazda, R.J. Barczyński, Solid State Ionics **271**, 86 (2015).
[15] M.V. Shankar, K.B.R. Varma, Mater. Sci. Lett. **15**, 858 (1996).
[16] Rahul Vaish, K.B.R. Varma, Adv. Sci. Lett. **2**, 319 (2009).
[17] N.A. Szreder, P. Kupracz, M. Prześniak-Welenc, J. Karczewski, M. Gazda, K. Siuzdak, R.J. Barczyński, Solid State Ionics **282**, 37 (2015).
[18] N. Syam Prasad, K.B.R. Varma, B. Lang Sidney, J. Phys. Chem. Solids **62**, 1299 (2001).
[19] M.V. Shankar, K.B.R. Varma, J. Non-Cryst. Solids **226**, 145 (1998).
[20] K.B.R. Varma, M.V. Shankar, G.N. Subbanna, Mater. Res. Bull. **31**, 475 (1996).
[21] M.V. Shankar, G.N. Subbanna, K.B.R. Varma, Bull. Mater. Sci. **18**, 931 (1995).
[22] N.Syam Prasad, K.B.R. Varma, J. Mater. Chem. **11**, 1912 (2001).
[23] M.V. Shankar, K.B.R. Varma, IEEE Proceedings on Applications of Ferroelectrics, 817 (1996).

[24] J. R. Macdonald, Solid State Ionics **133**, 79 (2000).

[25] A.K. Jonscher, Dielectric Relaxation in Solids, Chelsea Dielectrics, London, 1983.

[26] J.R. Macdonald, D.R. Franceschetti, in: J.R. Macdonald (Eds.), Impedance Scepctroscopy Emphasizing Solid Materials and Systems, (Wiley, New York, 1987) p. 98.

[27] S.R. Elliott, Adv. Phys. **36**, 135 (1987).

[28] N.F. Mott, J. Non-Cryst. Solids **1**, 1 (1968).

[29] A.K. Jonscher, Nature **267**, 673 (1977).

[30] A. K. Jonscher, The Universal Dielectric Response: A Review of Data their New Interpretation, London: Chelsea Dielectrics Group, 1978.

[31] W.K. Lee, J.F. Liu, A.S. Nowick, Phys. Rev. Lett. **67**, 1559 (1991).

[32] B.S. Lim, A.V. Vaysleyb, A.S. Nowick, Applied Phys. A **56**, 8 (1993).

[33] S. Kumar, K.B.R. Varma, Current Applied Physics **11**, 203 (2011).

[34] H. Jain, O. Kanert, Defects in Insulating Materials, Singapore: World Scientific, 1993, 274-294.